LANGMUIR

Article

New Insight into the Chemical Nature of the Plasmonic Nanostructures Synthesized by Reduction of Au(III) with Sulfide Species

Maria Ana Huergo, Lisandro J. Giovanetti, Mario Sergio Moreno, Christoph M. Maier, Felix G Requejo, Roberto C. Salvarezza, and Carolina Vericat

Langmuir, **Just Accepted Manuscript** • DOI: 10.1021/acs.langmuir.7b01168 • Publication Date (Web): 18 Jun 2017

ACS Publications

Langmuir is published by the American Chemical Society. 1155 Sixteenth Street N.W., Washington, DC 20036

New Insight into the Chemical Nature of the Plasmonic Nanostructures Synthesized by Reduction of Au(III) with Sulfide Species

M. A. Huergo[1], L. Giovanetti[1], M. S. Moreno[2], C. M. Maier[3], F. G. Requejo[1],

*R. C. Salvarezza[1], C. Vericat[1,]**

[1] Instituto de Investigaciones Fisicoquímicas Teóricas y Aplicadas (INIFTA), Universidad Nacional de La Plata – CONICET, Sucursal 4 Casilla de Correo 16, 1900 La Plata, Argentina.

[2] Centro Atómico Bariloche - S.C. de Bariloche, Argentina.

[3] Chair for Photonics and Optoelectronics, Department of Physics and Center for Nanoscience (CeNS), Ludwig-Maximilians-Universität München, Amalienstraße 54, 80799 Munich, Germany.

***Corresponding author**

Dr. Carolina Vericat

Email**: cvericat@inifta.unlp.edu.ar**

Phone: +54 221 4257430 ext. 194

ABSTRACT

We have studied the products of the controversial synthesis of $HAuCl_4$ with Na_2S, which include gold nanostructures (Au NSs) that absorb in the near-infrared (NIR) and are highly promising for photothermal therapies and other nanomedical applications. From high resolution transmission electron microscopy, X-ray absorption spectroscopy and small angle X-ray scattering we have found that only metallic gold nanostructures are formed as a result of this synthesis, with no detectable amount of gold sulfide or other oxidized gold species that could account for the NIR absorption. Different sulfur species are adsorbed on the Au NSs, mainly sulfides (monomeric sulfur) and polysulfides, similarly to what is found on planar gold surfaces, therefore precluding the idea that thiosulfate or other oxidized species are the actual reducing agents for Au(III) ions. The presence of strongly adsorbed S species, which are difficult to remove from the gold surface, is of great importance for their applications as regards toxicity and the use of post-functionalization strategies to anchor biomolecules and/or to increase circulation time after administration.

INTRODUCTION

Over the last few decades gold nanostructures (Au NSs) have attracted increasing interest because of the phenomenon of localized surface plasmon resonance (LSPR), which can decay either radiatively by light scattering, a process that finds multiple applications in the fields of optics and imaging, or non-radiatively as a result of the conversion of absorbed light to heat, a mechanism of dissipation of importance in several growing areas in nanomedicine, mostly for photothermal therapies and controlled drug release.[1-2] For many nanomedical applications of Au NSs, especially *in vivo* studies, it is desirable to work in the near-infrared (NIR) region of the spectrum (650-900 nm), as this light has small interference with tissue and interacts strongly with NSs that scatter and/or absorb in this region.[3]

Therefore, the development of synthetic methods of Au NSs, such as nanorods, nanoshells, nanotriangles and other anisotropic nanostructures of more complex shape, like nanostars, all of whom have LPSR in the NIR region, is currently an area of increasing interest.[4-5] Moreover, some anisotropic Au NSs are excellent substrates for surface-enhanced Raman scattering,[6] as they provide "hot spots" with no need to induce NS aggregation.[7-8] However, most syntheses are seed-mediated and as such involve multiple steps and use reagents and surfactants that are difficult to remove and are very toxic for cells, like CTAB.[6] Thus, the development of alternative methods to produce anisotropic NSs with LSPR in the NIR in a straightforward way and in the absence of surfactants is an important goal to achieve.[2]

In particular, the synthesis of Au NSs based on the reaction between Au(III) species (mostly $AuCl_4^-$ ions) and sulfide ions has attracted considerable interest because it yields in an easy way a variety of structures from spherical particles to triangular nanoplates, some of which absorb in the NIR region.[9-13] Different variations of the synthesis have been tried

and in all cases the same intriguing behavior has been observed: the peak in the NIR first shifts to higher wavelengths, while rapidly increasing in intensity, and then shifts to lower wavelengths.[9, 13]

Despite the interest in the synthesis, the nature of the NIR-absorbing nanostructures, in particular concerning their shape and chemistry, has been a matter of debate. Indeed, while some authors have proposed that they have a spherical core-shell structure, with a thin gold shell of variable thickness that surrounds a Au_2S core,[3, 9-10] this model has been challenged by others. In fact, Norman *et al.* support the idea that the origin of the redshift is the formation of aggregates of gold nanoparticles, even though this model eventually fails to describe the blueshift.[11,14] Also, it has been suggested that the NIR-absorbing nanostructures are made of amorphous Au_2S well mixed with crystalline Au.[15] A more plausible interpretation, however, is that non-spherical nanostructures (nanorods, nanotriangles, nanoplates, etc) are responsible for the NIR peak.[12, 16]

Very recently we have demonstrated - by single particle spectroscopy correlated with scanning electron microscopy of laser printed nanostructures - that nanotriangles are indeed responsible for the observed NIR absorption, with no evidence of absorption by spherical structures in that wavelength range.[13] Changes in the size and in the degree of truncation of the triangles can explain both their redshift and blueshift dynamics.[13] Although several authors presently accept that anisotropic Au NSs do contribute to the extinction peak in the NIR, some authors still believe that other NIR absorbing species, like the mentioned core-shell nanoparticles, can be formed from this synthesis or similar.[17-18] Moreover, the formation of a Au_2S phase has been reported by the same authors that supported the idea that nanotriangles were responsible for NIR absorption.[19]

It is thus clear that some unsolved questions remain in relation to this system. First, is gold sulfide really present in any of the structures produced in this synthesis, and if so, is it on the surface or in the bulk of the nanomaterials? Also, what are the sulfur species present on the surface of the Au NSs? Although some of these issues have been addressed in the past, we believe that some of the findings by other groups are not accurate. In particular, the possible formation of a Au_2S phase, either crystalline[9-10] or amorphous[15] and the real chemical nature of the sulfur species in the NSs[19] need to be further addressed.

In this work we have studied Au NS dispersions whose NIR peak lies at ≈ 850 nm, *viz.*, the optimal region for hyperthermia applications, by using complementary techniques: high resolution transmission electron microscopy, X-ray absorption spectroscopy and small-angle X-ray scattering. We have found that only metallic gold nanostructures are formed as a result of the synthesis, with no detectable amount of Au_2S or other oxidized gold species. The S species appear only at the nanoparticle surface and consist of a mixture of adsorbed sulfides (monomeric S), polysulfides and some elemental sulfur, similarly to what is found on planar gold surfaces upon sulfide adsorption.[20] The presence of strongly adsorbed reduced S species is of importance for nanomedical applications of these Au NSs as regards their toxicity[3, 21-22] and also for the use of post-functionalization strategies to anchor biomolecules and/or to increase circulation time after administration.[23-25]

EXPERIMENTAL SECTION

Synthesis of NIR-absorbing gold nanostructures:

Nanostructures were synthesized by reduction of $HAuCl_4$ with Na_2S following the two-step synthesis proposed by Zhou *et al.*[9] Briefly, 10 mL of 2 mM $HAuCl_4$ solution were quickly

mixed with 12 mL of freshly prepared 1mM Na_2S solution (pH = 10) at room temperature and without stirring. Ten minutes later, 2 mL of the sulfide solution were added, giving a total S/Au molar ratio equal to 0.7. The reaction was allowed to evolve, typically for 30-60 min, and was then arrested at different positions of the NIR peak by fast addition of 14 mL of the sulfide solution. In particular, for TEM, SAXS and XAS measurements this was done when the peak maximum reached a wavelength ≈ 850 nm during the blueshift. In some cases the arrested nanostructures were subsequently purified by centrifugation (10-30 min at 7000 rpm), followed by the replacement of the supernatant with ultrapure water. The evolution of the synthesis and the stability of the nanostructures were studied by UV-vis spectroscopy by means of a Lambda 35 spectrophotometer (Perkin Elmer).

Synthesis of S-capped gold nanoparticles:

Gold nanoparticles about 20 nm in diameter were synthesized following the method of Ref. 26. Briefly, 10 mL of a 38.8 mM sodium citrate solution were added to 100 mL of a boiling 1 mM $HAuCl_4$ solution and stirred for 30 minutes. The as-synthetized Au NPs were capped with S by addition of 8.4 mL of 6 mM Na_2S solution, giving a S/Au molar ratio of 0.5. Purification was carried out as described for the gold nanostructures.

Transmission electron microscopy:

TEM specimens were prepared by dropping the samples on an ultrathin carbon film (Ted Pella, Inc). Selected area electron diffraction patterns and high resolution transmission electron microscopy (HRTEM) images were acquired using a Tecnai F20 G^2 transmission electron microscope operated at room temperature and 200 kV. Images were analyzed using the Digital Micrograph program (Gatan Microscopy Suite®). We have used the Fast

Fourier Transform of windowed regions for the local measurement of the spacings observed in the image. Spacings measured in the FFT are the reciprocal of those in the image.

SAXS experiments:

SAXS measurements were performed using a XEUSS 1.0 from XENOCS equipment equipped with a 2D photon counting pixel X-ray detector Pilatus 100k (DECTRIS, Switzerland). The scattering intensity, *I(q)*, was recorded in the range of the momentum transfer $0.04 < q < 1.4$ nm^{-1}, where $q = {}^{4\pi}/_{\lambda}\, Sin(\theta)$, 2θ is the scattering angle and λ = 0.15419 nm is the weighted average of X-ray wavelength of the $Cu\text{-}K_{\alpha 12}$ emission lines. All measurements were carried out using glass capillary as sample holder and all reported data were corrected for the solvent scattering and processed using standard procedures.

Au-L_3 edge XANES experiments:

XAFS experiments at the Au-L_3 edge (11919 eV) were performed at the XAFS-2 beamline of the LNLS (Campinas, Brazil) which is equipped with a Si(111) double crystal monochromator. The X-ray beam is vertically collimated giving a spot at the sample of about 0.2 mm × 3 mm. All experiments where performed in transmission mode adjusting the gas mixtures in the chambers for the required energy range. The energy calibration was monitored by measuring a thin Au film simultaneously with the sample, through a third ionization chamber. XAFS data were processed by standard methods by using ATHENA software, which is part of the IFFEFIT package.[27] Samples were measured in solution using

a sample holder consisting of plastic pieces, about 1 cm thick, sealed with Kapton® windows.

S-K edge XANES experiments:

S-K edge XANES experiments were performed at the SXS beamline at the LNLS (Campinas, Brazil),[28] which is equipped with a InSb(111) double crystal monochromator with slit aperture of 1 mm, giving an energy resolution of about 0.6 eV. Either sodium thiosulfate in solution or as a solid was used as reference, since both spectra are identical. The photon energy was calibrated by assigning the value 2481.5 eV to the highest maximum of $Na_2S_2O_3$ (corresponding to the so-called inner sphere), in accordance with the criteria previously reported by Vairavamurthy.[29] All liquid samples were prepared by drop casting on carbon disks (Ted Pella Inc). All reported experiments in the S K-edge were measured in ultra-high vacuum (10^{-7} torr). Absorption spectra for each sample was recorded in fluorescence mode following the intensity of S-$K_{\alpha 1,2}$ emission lines (2309.5 and 2308.4 eV, respectively).

RESULTS AND DISCUSSION

Typical sequential UV-vis spectra of the reaction mixture (Figure 1a), acquired as the synthesis originally proposed by Zhou *et al.*[9] (S/Au molar ratio = 0.7) proceeds, show two absorption peaks whose intensities increase with time, one that remains fixed at $\lambda \approx$ 525 nm and a second one in the near-infrared (NIR) region, which first shifts to higher wavelengths (up to approximately 1000 nm) and then shifts to lower wavelengths. Sulfide/gold ratios > 1 give spectra which lack completely from both absorption peaks.[12] The evolution of the

synthesis can be arrested at any time by quick incorporation of an additional aliquot of Na_2S solution,[30] as already described.[13] These arrested samples are stable for months, in contrast to non-arrested ones, which generally aggregate irreversibly within a few days. Unless otherwise noted, all dispersions in this work were arrested at about 850 nm during the blueshift, as this is the wavelength region of interest for hyperthermal applications.

Figure 1b shows a typical transmission electron microscopy (TEM) image of the arrested as-synthesized dispersion that contains all the observed nanostructures: nanotriangles with different degree of truncation (most with side length about 80 nm, see Fig. S1a) in the Supporting Information), nanoplates, large "spherical-like" nanoparticles (NPs) with typical sizes 15-40 nm (Figure S1b)) and small nanoparticles (diameter < 10 nm) which can be largely removed by purification. From the analysis of many TEM and atomic force microscopy (AFM) images it can be concluded that nanotriangles and nanoplates represent about 20% of the large nanostructure population (*i.e.*, all the nanostructures excluding the small nanoparticles) (Figure S1c) and Ref.13). AFM height analysis (see Figure S2 in the Supporting Information) confirms that these Au NSs are plate-like (average height is ≈ 9 nm) and that the large "spherical-like" nanoparticles termed are isotropic. Other authors have obtained similar structures and proportions with the same two-step synthesis[9] and with a similar synthesis in one step.[12,15] Also, we have recently shown that nanotriangles whose NIR peak appears at 800-850 nm have a higher degree of edge truncation compared to those at 1000-1100 nm.[13]

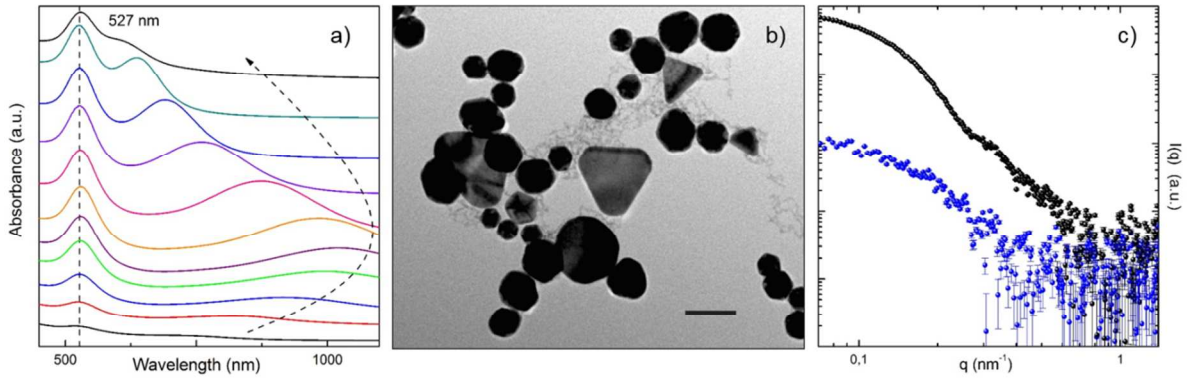

Figure 1. (a) Sequential UV visible spectra showing the evolution of the two absorption peaks. (b) TEM image of the as-synthesized dispersion arrested at 850 nm. The scale bar corresponds to 50 nm. (c) SAXS curves of an arrested Au NS sample (black) and of the supernatant obtained after centrifugation (blue).

In order to analyze the proportion of large Au NSs (nanotriangles, nanoplates and large isotropic NPs) compared to that of small NPs we have performed small angle X-ray scattering (SAXS) experiments over samples of arrested Au NSs and also of the corresponding supernatants obtained after centrifugation. TEM images and UV-vis spectra (data not shown) suggested that most large NSs remain in the pellet, while the supernatant is mainly composed of small Au NPs.

Figure 1c shows a significant difference between both samples (the "whole" sample and the supernatant), as evidenced by the intensity and the slope at smaller q values ($q \rightarrow 0$). Keeping in mind that the intensity extrapolated at $q = 0$ is proportional to the number of objects, and to the square of the volume of the illuminated objects, it is possible to conclude that the population of larger particles is notoriously diminished in the supernatant due to the smaller intensity at $q = 0$ in the original solution compared to the supernatant. Additionally, the decrease in the slope value at smaller q values ($q \rightarrow 0$), reveals the presence of a

population of much smaller particles in average size in the supernatant and confirms that most large Au NSs (nanotriangles, nanoplates and large isotropic nanoparticles) are retained in the pellet. To obtain a quantitative estimation of the average size of the particles, we have analyzed the SAXS scattering curve at very small scattering angles following a standard formalism derived by Guinier,[31] which gives an estimation of the average radius of gyration (*Rg*) (see Figure 1c and Figure S3 and Table S1 in the Supporting Information). Moreover, the Gaussian shape of the curves in the small *q* region precludes the possibility of agglomeration for all the studied samples under analysis, further discarding nanoparticle agglomerates as responsible for the NIR LSPR peak, in contrast to the model proposed by some authors.[11,14]

In order to determine the relative fraction of small nanoparticles in each sample, we have made use of the *Q* invariant that can be obtained from a SAXS curve and which gives an estimation of the volume fraction occupied by the nano-object in solution (see the Supporting Information). From the comparison of the *Q* values of both samples we can conclude that the fraction in volume of the small Au NPs is below 5% (see Figure S4 and Table S2 in SI). As it is possible to see from TEM and SAXS results, these small nanoparticles contribute in a negligible fraction in volume thus assuring that the analyses of gold and sulfur species from X-ray absorption spectroscopy (XAS) experiments (see below) are representative of their chemical state in large Au NSs (at least 95% of the atoms in all the analyzed samples correspond to these NSs).

To get more insight into the structure of the different NSs obtained in the synthesis, and to avoid average results, we have made an extensive analysis of the HRTEM images by means of the Fast Fourier Transform (FFT) of each whole single particle and smaller regions of each particle, as indicated in Figure 2. This local analysis, in contrast to average diffraction

techniques, is particularly convenient in the case of nanotriangles because of their scale. In this way we attempt to detect if a crystalline Au_2S phase (or any other oxidized phase) is present in any of the different nanostructures, as previously reported by some authors.[9, 32] The images in Figure 2a and 2b show two triangular nanoplates with different degree of truncation. In both cases the FFT showed the allowed {220} reflections and the forbidden 1/3{422} reflections of metallic gold already reported for this type of structures in a <111> incidence (see corresponding panels in Figure 2),[16] the latter arising from the formation of stacking faults of the fcc lattice.[33]

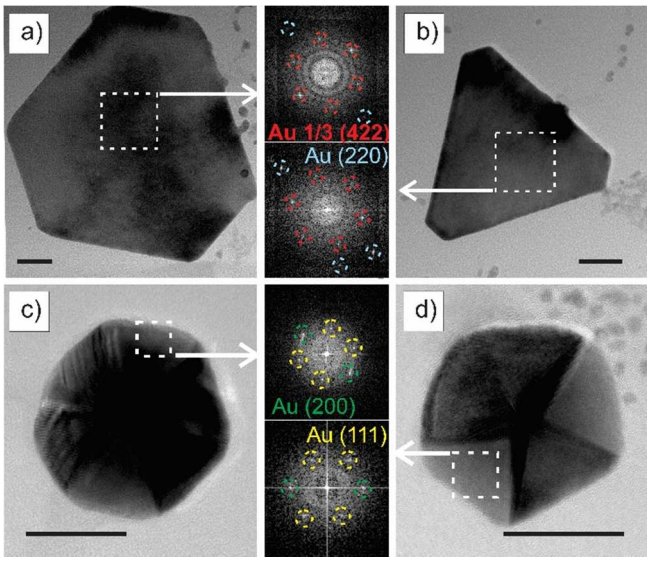

Figure 2. High resolution TEM images of the different typical Au NSs obtained in the synthesis with the corresponding FFT pattern for the region indicated by the box: (a) nanoplate; (b) truncated nanotriangle; (c) typical icosahedrical nanoparticle; (d) typical decahedrical nanoparticle. In all the images the scale bar corresponds to 20 nm.

On the other hand, large isotropic nanoparticles show multiple twinning (Figure 2c and 2d). Some of them have a close to hexagonal shape, presumably because of an icosahedral morphology, and exhibit six twin planes (Fig 2c). Also, a small number of the large

nanoparticles have a 5-fold axis and can be regarded as decahedra (Figure 2d).[34] A similar analysis based on the FFT of regions indicated by dash squares in Figure 2c and 2d show a quasi- hexagonal array of spots that corresponds to the (111) and (200) plane distances for a gold fcc structure. Although these particles have been considered as the candidates to Au_2S core-Au shell nanoparticles by those authors who claim that these are the structures responsible for NIR peak,[9-10] the spots in the FFT can be accounted for only in terms of reflections of metallic gold, with no contribution from Au_2S or other phases.[35]

Finally, small nanoparticles also show typical Au reflections (see Figure S5 in the Supporting Information). Thus, for all the analyzed nanostructures we have found reflections that correspond only to gold and some additional forbidden reflections due to growth defects (twin planes). In other words, HRTEM results indicate that all the structures formed are composed of metallic gold, with no significant traces of crystalline Au_2S or other oxidized gold species, which in fact would be thermodynamically unstable in water at the low pH of the synthesis (between 2 and 3).

For a more detailed understanding on the bulk structure of the synthesized species, we have performed XAS experiments, which yield chemically selective information (in our case for Au and S) not only from the surface of the material but also from the bulk. Au-L_3 X-ray near edge structure (XANES) measurements of the arrested Au NS dispersions were performed in a liquid cell in order to analyze the oxidation state(s) of gold in the nanomaterials. A general inspection of the main features of the spectrum in Figure 3a (blue line) indicates the predominant metallic state of Au in the gold nanostructures. Indeed, it clearly shows the similarity between the Au NS sample and a gold metallic foil used as Au(0) reference (black line) and the remarkable differences with the Au(I) (red line) and Au(III) (green line) reference compounds. A more detailed comparison of both spectra

(Figure 3b) confirms the complete agreement between the spectrum of the sample and that of the metallic reference. Additionally, Au(I) or Au(III) oxidation states can be ruled out based on the absence of the white line at about 11923 eV (see red and green lines in Figure 3a). Only a slight variation in the difference spectrum can be observed around 11496 eV (see inset in Figure 3b) that corresponds to the maximum resonance peak at the region of multiple scattering process and which can be attributed to size and/or surface effects due to the interaction between Au and S atoms, the latter belonging to the capping molecules. This is in good agreement with our TEM results, further confirming the absence of a Au_2S phase, either crystalline[9] or amorphous,[15, 36] and thus precluding the existence of core-shell nanoparticles. Moreover, it confirms that no Au_2O_3 or any other Au(III) species are formed, as expected from their low thermodynamic stability in aqueous solutions.[37-38]

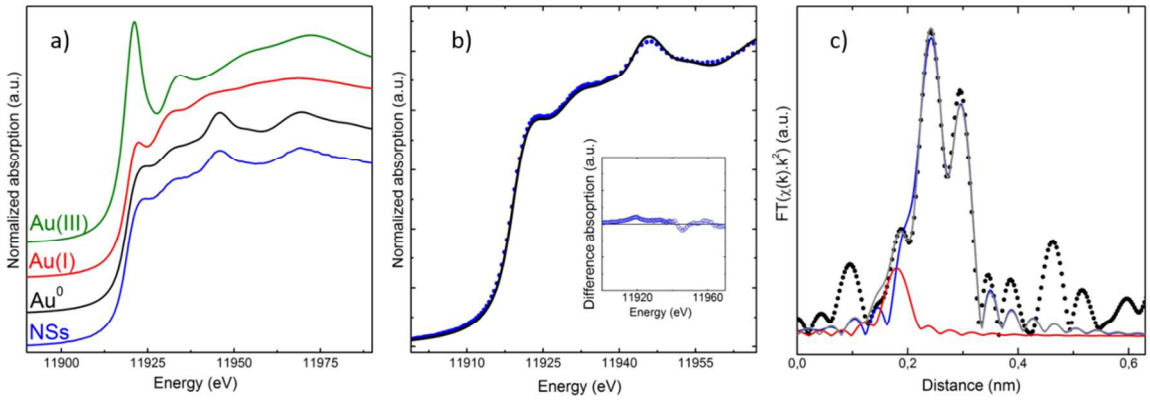

Figure 3.(a) Au-L_3 XANES spectra of as-prepared, arrested sample recorded in solution (blue line); metallic Au foil (black line). Reference compounds were also measured for comparison: Au(III) chloride (green line) and Au(I) chloride (red line). (b) Detail of the Au-L_3 XANES spectra corresponding to metallic Au foil (black line) and Au NS sample (blue circles). The inset shows the difference spectrum. The small deviation can be attributed to the S-Au interaction at the Au NS surface. (c) *Experimental Fourier*

Transform of EXAFS oscillation of the arrested Au NS sample (dotted line) and the corresponding fitting (full grey line). Blue and red full lines represent the Au-Au and Au-S contributions, respectively.

In order to analyze the interaction between Au and S elements, we have performed extended X-ray absorption fine structure (EXAFS) experiments at the Au L_3-edge. Figure 3c shows the fitted Fourier Transform corresponding to the EXAFS signal of the same Au NS sample considered for XANES. Even if there is high polydispersity of the sample, both in size and in shape, and the S content is very low in comparison to Au, this experiment allows a tentative quantification of the Au/S ratio and the determination of possible Au-S species. Thus, from the fitted average coordination values *N* (Table 1), we can infer that only 3% of the atoms around Au, in average, are S atoms (*i.e.* $N_{Au\text{-}Au}/N_{Au\text{-}S}$). This percentage indicates that, if any Au_xS_y species were present, they would represent a negligible proportion. A more reasonable hypothesis is that S atoms are only located at the surface of the Au NSs and do not form any type of gold sulfide, in agreement with Au-L_3 XANES results. The Au-S fitted distance of 0.224(5) nm (Table 1) is somewhat lower than the 0.233 nm value reported, for instance, for adsorbed alkanethiols on Au NPs.[39] The origin of this lower value is probably due to the effect of the variety of Au-S bond lengths present in the different sulfur species adsorbed on Au, as it will be shown below.

Samples with similar S/Au ratio (0.6-0.7) had already been studied by EXAFS by others,[19] although the fitting strategy did not include Au-S coordination in their analysis. Because they did not indicate the anti-transformed region, it was not possible to compare both experimental results and the probable inclusion of the corresponding Au-S coordination

sphere in their results (that could be observed also in their experimental data as a small contribution in the Fourier Transform below 2 Å).

Coordination shell	*N*	*D* / nm	σ^2 / nm^2	E_0 / eV
Au-Au	8.5 (9)	0.284 (4)	0.000072 (9)	4.2 (6)
Au-S	0.3 (2)	0.224 (5)	0.00001 (5)	4.2 (6)

Table 1: Fitted parameters for EXAFS signal detailing each of the coordination shells showed in Figure 3c. N is the average coordination number, D the interatomic distance, σ^2 the Debye-Waller factor and E_0 the energy shift. Errors are between brackets.

Because EXAFS fitted parameters represent an average signal over all illuminated atoms that may be part of different species, it is difficult to assign univocally the origin of the obtained values. Previous studies of similar Au NS samples were not conclusive as regards the origin of Au-S bonds. The absence of Au-S distances characteristic of a Au_2S phase (0.231 nm) (see for example Ref. 40) is in agreement with previous data,[11] although these authors concluded that gold nanoparticle aggregates were responsible for NIR absorption, a model that is not consistent with the observed shifts in UV-vis spectra and which can be further discarded from our SAXS results. Another work proposed the existence of Au_2S into Au particles;[15] however their analysis was based on an incorrect comparison with reference samples, as their S-K XANES reference spectra do not agree with those reported in the literature for the different S species present in the sample.

In summary, the existence of a Au_2S phase, either crystalline or amorphous, can be ruled out in our samples from Au-L_3 XANES and EXAFS experiments, and it is clear that S species are located on the surface of the nanostructures. This result is also of relevance in relation to the discussion of whether a gold sulfide phase is feasible as a result of the reaction of sulfur species with Au(111) surfaces.[41] The fact that, even if we put sulfide /polysulfide ions in contact with Au(III) ions, only metallic gold nanostructures are formed clearly shows the thermodynamic instability of oxidized gold in contact with reduced S species, as already reported.[20]

The next point to address is the chemical nature of these adsorbed S species, an issue that has received relatively little attention in the past. It has been pointed out by some authors that the actual reducing agent of the Au(III) ions in the present synthesis are S-O species, most probably thiosulfate ions, which are formed as a result of polysulfide ion oxidation in air, as sulfide ions easily form polysulfides in aqueous solutions.[42] This statement was supported by the fact that the synthesis is improved, *i.e.*, the ratio of the NIR to 520 nm LSPR peaks is enhanced, when aged Na_2S solutions are used.[14] However, in our case we have found that replacing freshly prepared sulfide solutions by aged ones does not enhance the NIR peak. In line with the model of Ref. 14, several groups have performed the synthesis directly using $Na_2S_2O_3$ as the reducer and have obtained similar nanostructures.[14, 17-18] The oxidation product of thiosulfate upon Au(III) reduction would be either sulfate or sulfite species.[2, 17]

In order to shed light on the nature of the adsorbed S species on the gold nanostructures produced in the present synthesis, we have performed XANES spectroscopy experiments at the S K-edge on different Au NS samples (Figure 4). We have studied the Au NSs produced by the synthesis in different conditions: (1) non-arrested; (2) arrested without

purification by centrifugation and (3) arrested and then purified. We have also included for comparison the spectrum of a sample consisting of purified S-capped Au NPs, *viz.* nanoparticles that were post-functionalized with sulfide.[26] As mentioned above, SAXS results imply that about 95% of the XAFS signal corresponds to nanotriangles and large Au NPs. In all cases the samples were prepared by drop casting and then rinsed with water to remove free S species present in the reaction mixture.

We have chosen sodium thiosulfate as reference compound because it has two well-defined peaks at 2472.4 eV and 2481.5 eV (see Figure 4) that correspond to the outer and inner S atoms of the molecule, respectively.[43] All the samples present two main features: a broad peak in the region of low oxidation states centered about 2473 eV, and another one in the region corresponding to oxidized S species, centered about 2483 eV. Taking into account the spectrum of thiosulfate used as reference and different S-K XANES studies reported elsewhere,[29, 43-44] we can assign the region at 2470-2475 eV to different reduced S species (sulfide, polysulfide species and elemental sulfur) and that at E > 2482 eV to sulfates.

As regards the presence of sulfate in the samples, this could in principle be generated either as a result of the oxidation of sulfide upon reduction of the Au(III) species, as proposed for a very similar synthesis,[19] or as the product of thiosulfate oxidation.[2, 17] However, sulfate is also present in the S-capped Au NP samples, where no reaction between sulfide and gold ions takes place. Therefore, we propose that in our case sulfate species are produced by oxidation of the reduced sulfur species during the long time exposure of the Au NS samples to the ambient conditions as a result of the drop casting procedure. Interestingly, the sulfate peak markedly decreases as Au NS dispersions are successively purified, thus indicating that sulfate ions are mostly present in solution and also possibly physisorbed on the gold

nanostructures. In contrast, the intensity of the reduced S region remains almost constant after purification, suggesting that most of these species are chemisorbed on gold.

In order to gain more insight into the chemical nature of the S species present in the different samples, we have fitted the region of the XANES spectra that corresponds to the reduced S species (with a maximum at about 2473 eV). Figure 5 shows this region for the different samples considered in Figure 4. In all cases the background was fitted by an arctg function and the peaks were represented by Gaussian functions (details of the results of the fitting are shown in Table S3 in the Supporting Information); spectra were adjusted with three components. The peak of the sodium thiosulfate sample, that appears at lower energy (Figure 5a), was used as a reference for the component assigned to sulfide species (peak 1), which are adsorbed on Au as monomeric S. The remainder of the area corresponds to two additional curves at higher energies (peaks 2 and 3), which we have assigned to polysulfide species and elemental sulfur, respectively.[29, 45] It is worth to mention that this assignation is in agreement with the components in X-ray photoelectron spectra for the same S-capped Au NPs used as reference[46] and, in turn, with S self-assembled monolayers on Au(111) prepared from sulfide solutions.[20]

In this perspective, we can also better understand the somehow low value for the Au-S distance obtained from EXAFS data for the arrested sample (Figure 3c) from the presence of the different reduced S species on the gold surface, mostly monomeric S and adsorbed polysulfides, in addition to some elemental S, as found on planar Au substrates.[20] The Au-S bond length distances for monomeric S adsorbed at 3-fold hollow sites is about 2.28 Å,[47-48] close to the average value obtained from the fitting of the EXAFS curves.

From the fitting and the analysis of the peak area ratio of sulfide (peak 1) to the total reduced S species (sum of the areas of peaks 1, 2 and 3) we can estimate the relative

concentration of sulfide species for the different samples (Figure 5f). In the first place, the spectrum of the S-capped Au NP sample used for comparison has about 40% of sulfide species (Figure 5b and 5f) adsorbed as monomeric S, in line with previous XPS results for these nanoparticles,[46] which also coincide with those for S SAMs on Au(111) (although in the case of planar surfaces the elemental S component can be generally removed by thorough rinsing).[20] This is in agreement with the fact that the adsorption of sulfides is stronger than that of polysulfides on gold surfaces.[20, 49]

For non-arrested Au NS dispersions both peaks 2 and 3 increase with respect to peak 1, giving a lower proportion of sulfides (about 20%) (see Figures 5c and 5f). This fact can be explained by considering that elemental S is formed through the reaction already proposed for the same synthesis[10]

$$2\ AuCl_4^- + 3\ HS^- \rightarrow 2\ Au + 3\ S + 3\ H^+ + 8\ Cl^- \qquad [1]$$

Then, some of the elemental S can react with sulfide ions to yield polysulfides on the Au NS surface.[50-51] On the other hand, for sulfide-arrested, non-purified Au NS samples there is about 50% of sulfide (Figures 5d and 5f): this can be accounted for by the higher affinity of sulfide for metallic gold, therefore possibly displacing some of the polysulfides and elemental S from the nanostructure surface. Also, it is possible that some of the sulfide ions are not adsorbed on the gold surface. Finally, for purified arrested samples (Figures 5e and 5f) the polysulfide peak has increased while the other two decrease (the proportion of sulfide is about 25%), thus confirming that some sulfide species in the non-purified sample were not adsorbed. More important, this spectrum is very similar to that for S-capped AuNPs, and leads us to conclude that practically all reduced S species in the purified Au NS samples are chemisorbed.

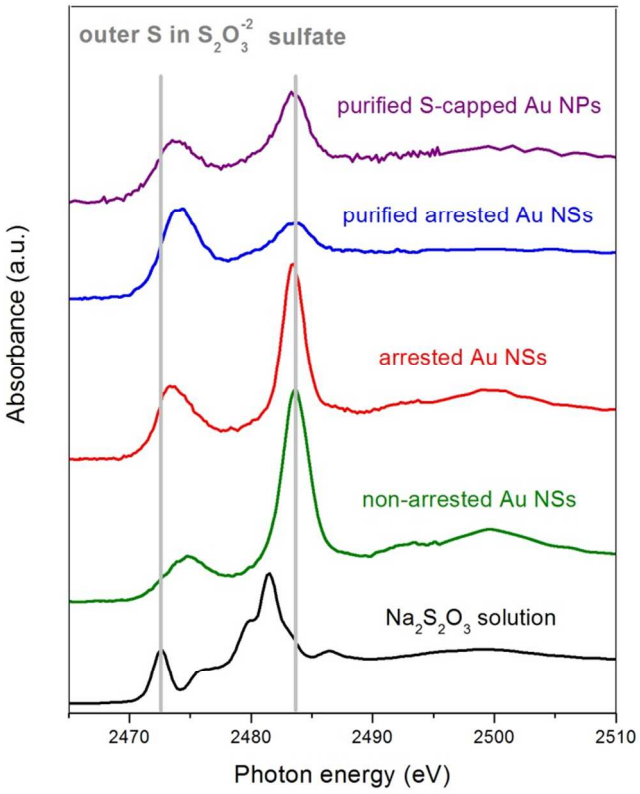

Figure 4: S-K XANES spectra of the different samples: reference thiosulfate solution (black); non-arrested Au NSs (green); non-purified arrested Au NSs (red); purified arrested Au NSs (blue) and purified S-covered Au NPs used as a reference (violet).

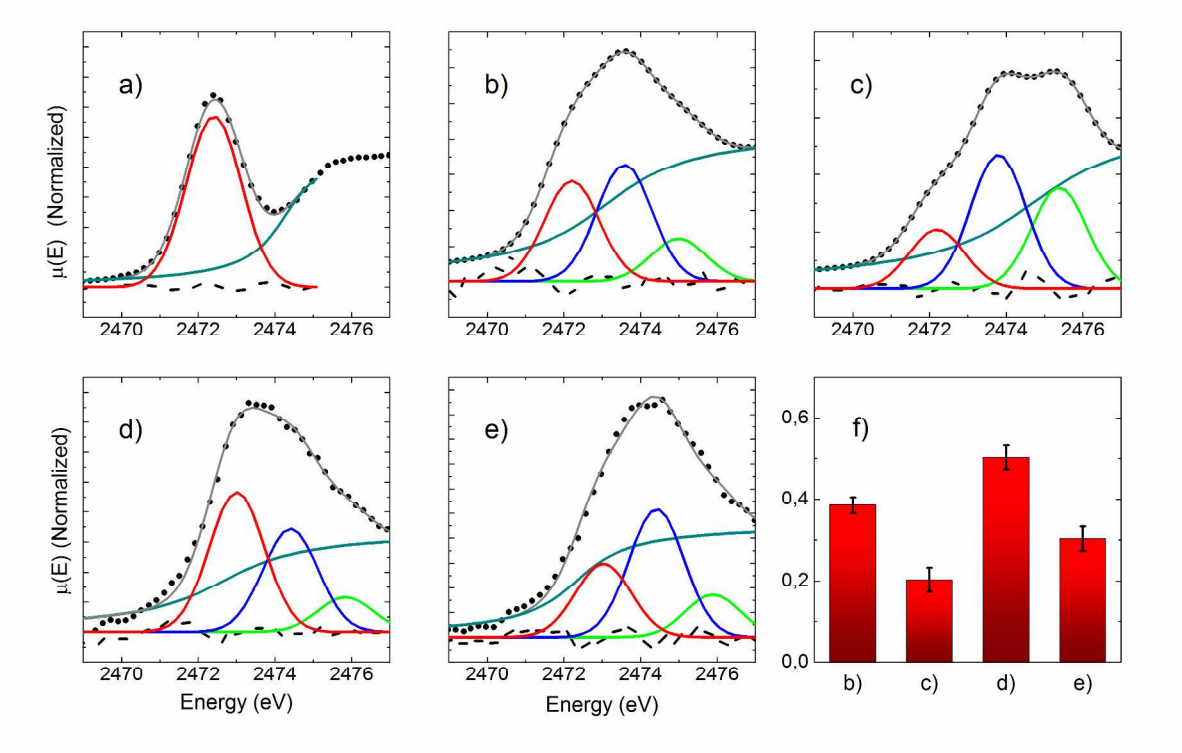

Figure 5. (a)-(e) XANES fitting of the region of reduced S species of the samples in Figure 4: a) thiosulfate solution; b) purified S-capped Au NPs; c) non-arrested Au NSs; d) non-purified arrested Au NSs, e) purified arrested Au NSs. Peak 1: sulfides (red); peak 2: polysulfides (blue); peak 3: elemental S (green). f) Sulfide proportion calculated as the area of peak 1 divided by the sum of the areas of peaks 1, 2 and 3 for samples in b), c), d) and e).

The knowledge of the nature of the species that are formed and which remain adsorbed on the gold nanostructures is relevant for several reasons.[52] First, for any *in vitro* or *in vivo* biomedical applications it is essential that the surface coating of the nanostructures is biocompatible and non-toxic.[21-22, 53] In addition, for *in vivo* applications it is necessary that Au NSs are not easily eliminated from the systemic circulation by the mononuclear phagocyte system and this is achieved by the use of hydrophilic coatings, like polyethylene

glycol.[54] Functionalization with PEG is usually performed by addition of thiolated PEG, as thiols chemisorb on gold through the S atoms. Also, the same strategy is used to anchor a drug, a vector biomolecule, or a dye label on the gold surface.[23, 55-56] Thus, it is important to know if the initial surface coating of the nanostructures can be effectively exchanged by thiol molecules.

In this sense, it is important to assess the role of the S coating on the extinction spectra of the nanotriangles if this has to be removed for biocompatibility or postfunctionalization purposes. The quantitative effect of a particular coating, or adsorbed species, on the intensity and position of the LSPR peaks of nanostructures is not easy to predict because it depends on the refractive index of the coating, its thickness and also on the LSPR strength and its wavelength.[57-59] In order to address this point we performed electrodynamical simulations using a finite-difference time-domain (FDTD) method (see details and Figure S6 in the Supporting Information). Our results clearly show that the absorption, scattering and extinction cross sections are not affected by a S monolayer, and thus the plasmonic properties of the nanotriangles will not be significantly modified as a result of the removal of the S coating.

Finally, for hyperthermia and other applications that require illumination with laser light, it is important that the chosen Au NS coating resists the temperature increase upon heating, as this can cause the undesired release of the species of interest, or can even induce changes in nanostructure shape as a result of surface diffusion.[13, 60-62]

SUMMARY AND CONCLUSIONS

Our combined HRTEM, XAS and SAXS studies shows that the synthesis of Au NSs by reaction of Au(III) with sulfide produces only metallic gold nanostructures, with no

detectable amount of Au_2S or any other oxidized gold species. As previously demonstrated,[13] nanotriangles with different degree of truncation and nanoplates (even if present in a lesser proportion) are the only structures responsible for the LSPR peak in the NIR. More importantly, we have found that the S species adsorbed on all Au NSs are mostly polysulfides and monomeric S, with some elemental S that is formed in the reduction of the Au(III) species. Thiosulfate species are not formed on the nanostructure surface, and some sulfate species appear as a result of the preparation of the samples, but mostly correspond to the oxidation of reduced S species in the solution. Thus, the interface in these Au NSs is similar to that in S self-assembled monolayers of S on planar gold surfaces.

These findings have implications for the use of these NIR-absorbing Au NSs for nanomedical applications if post-functionalization of their surface is to be carried out in order to increase their biocompatibility and/or to anchor a drug, a vector biomolecule or a dye label. Certainly, the presence of strongly adsorbed S species, like sulfides and polysulfides, should be carefully considered as they are difficult to remove by simple ligand exchange methods.[63-64] Also, this knowledge can contribute to shed light on some controversial aspects about the nature of the interface of self-assembled monolayers of S and S-bearing molecules (especially thiols), both on gold planar surfaces and gold nanoparticles.[41, 46, 65]

ASSOCIATED CONTENT

Supporting Information. The following material is included: size and shape histograms of the nanostructures; AFM image of the Au nanostructures; Guinier and Kratky plots of the

SAXS data, together with details on the analysis and the obtained data; HRTEM image of small Au nanoparticles; S K-edge XANES data for the different samples; FDTD calculations for a gold nanotriangle with and without S capping. This material is available free of charge *via* the Internet at http://pubs.acs.org.

AUTHOR INFORMATION

Corresponding Author

* CV: cvericat@inifta.unlp.edu.ar

Author Contributions

The manuscript was written through contributions of all authors. All authors have given approval to the final version of the manuscript.

ACKNOWLEDGEMENTS

This work has been financially supported by ANPCyT (PICT 2012-0836, 2010-2554, 2012-1136 and 2015-2285) and CONICET (PIP 112-201201-00093 and 112-201101-01035) from Argentina and DFG (grant SFB1032) from Germany. Partial support by Laboratório Nacional de Luz Síncrotron (LNLS) under proposals SXS 20150180 and XAFS2 20160225 is acknowledged. Authors would also like to thank Dr. Theobald Lomueller and Prof. Joachim Rädler from Ludwig-Maximilians-Universität München, Germany.

REFERENCES

1. Jain, P. K.; Huang, X.; El-Sayed, I. H.; El-Sayed, M. A. Noble Metals on the Nanoscale: Optical and Photothermal Properties and Some Applications in Imaging, Sensing, Biology, and Medicine. *Acc. Chem. Res.* **2008,** *41*, 1578-1586.

2. Pelaz, B.; Grazu, V.; Ibarra, A.; Magen, C.; del Pino, P.; de la Fuente, J. M. Tailoring the Synthesis and Heating Ability of Gold Nanoprisms for Bioapplications. *Langmuir* **2012,** *28*, 8965-8970.

3. Gobin, A. M.; Watkins, E. M.; Quevedo, E.; Colvin, V. L.; West, J. L. Near-Infrared-Resonant Gold/Gold Sulfide Nanoparticles as a Photothermal Cancer Therapeutic Agent. *Small* **2010,** *6*, 745-752.

4. Tréguer-Delapierre, M.; Majimel, J.; Mornet, S.; Duguet, E.; Ravaine, S. Synthesis of Non-spherical Gold Nanoparticles. *Gold Bull.* **2008,** *41*, 195-207.

5. Li, N.; Zhao, P.; Astruc, D., Anisotropic Gold Nanoparticles: Synthesis, Properties, Applications, and Toxicity. *Angewandte Chemie International Edition* **2014,** *53* (7), 1756-1789.

6. Scarabelli, L.; Coronado-Puchau, M.; Giner-Casares, J. J.; Langer, J.; Liz-Marzán, L. M. Monodisperse Gold Nanotriangles: Size Control, Large-Scale Self-Assembly, and Performance in Surface-Enhanced Raman Scattering. *ACS Nano* **2014,** *8*, 5833-5842.

7. Shiohara, A.; Wang, Y.; Liz-Marzán, L. M. Recent Approaches Toward Creation of Hot Spots for SERS Detection. *J. Photoch. Photobio. C* **2014,** *21*, 2-25.

8. Tian, F.; Bonnier, F.; Casey, A.; Shanahan, A. E.; Byrne, H. J. Surface Enhanced Raman Scattering with Gold Nanoparticles: Effect of Particle Shape. *Anal. Methods* **2014,** *6*, 9116-9123.

9. Zhou, H. S.; Honma, I.; Komiyama, H.; Haus, J. W. Controlled Synthesis and Quantum-size Effect in Gold-coated Nanoparticles. *Phys. Rev. B* **1994,** *50*, 12052-12056.

10. Averitt, R. D.; Sarkar, D.; Halas, N. J. Plasmon Resonance Shifts of Au-Coated Au2S Nanoshells: Insight into Multicomponent Nanoparticle Growth. *Phys. Rev. Lett.* **1997,** *78*, 4217-4220.

11. Norman, T. J.; Grant, C. D.; Magana, D.; Zhang, J. Z.; Liu, J.; Cao, D.; Bridges, F.; Van Buuren, A. Near Infrared Optical Absorption of Gold Nanoparticle Aggregates. *J. Phys. Chem. B* **2002,** *106*, 7005-7012.

12. Mikhlin, Y.; Likhatski, M.; Karacharov, A.; Zaikovski, V.; Krylov, A. Formation of Gold and Gold Sulfide Nanoparticles and Mesoscale Intermediate Structures in the Reactions of Aqueous $HAuCl_4$ with Sulfide and Citrate Ions. *Phys. Chem. Chem. Phys.* **2009,** *11*, 5445-5454.

13. Huergo, M. A.; Maier, C. M.; Castez, M. F.; Vericat, C.; Nedev, S.; Salvarezza, R. C.; Urban, A. S.; Feldmann, J. Optical Nanoparticle Sorting Elucidates Synthesis of Plasmonic Nanotriangles. *ACS Nano* **2016,** *10*, 3614-3621.

14. Schwartzberg, A. M.; Grant, C. D.; van Buuren, T.; Zhang, J. Z. Reduction of $HAuCl_4$ by Na_2S Revisited: The Case for Au Nanoparticle Aggregates and Against Au_2S/Au Core/Shell Particles. *J. Phys. Chem C* **2007,** *111*, 8892-8901.

15. Tan, M. C.; Ying, J. Y.; Chow, G. M. Structure and Microstructure of Near Infrared-absorbing Au–Au_2S Nanoparticles. *J. Mater. Res.* **2007,** *22*, 2531-2538.

16. Diao, J. J.; Chen, H. Near Infrared Surface Plasmon Resonance of Gold Tabular Nanostructures in the $HAuCl_4$–Na_2S Reaction. *J. Chem. Phys.* **2006,** *124*, 116103.

17. Zhang, G.; Jasinski, J. B.; Howell, J. L.; Patel, D.; Stephens, D. P.; Gobin, A. M. Tunability and Stability of Gold Nanoparticles Obtained from Chloroauric Acid and Sodium Thiosulfate Reaction. *Nanoscale Res. Lett.* **2012,** *7*, 337.

18. Patel, D.; James, K. T.; O'Toole, M.; Zhang, G.; Keynton, R. S.; Gobin, A. M. A High Yield, One-pot Dialysis-based Process for Self-assembly of Near Infrared Absorbing Gold Nanoparticles. *J. Colloid Interface Sci.* **2015,** *441*, 10-16.

19. Mikhlin, Y.; Likhatski, M.; Tomashevich, Y.; Romanchenko, A.; Erenburg, S.; Trubina, S. XAS and XPS Examination of the Au–S Nanostructures Produced via the Reduction of Aqueous Gold(III) by Sulfide Ions. *J. Electron Spectros. Relat. Phenomena* **2010,** *177*, 24-29.

20. Lustemberg, P. G.; Vericat, C.; Benitez, G. A.; Vela, M. E.; Tognalli, N.; Fainstein, A.; Martiarena, M. L.; Salvarezza, R. C. Spontaneously Formed Sulfur Adlayers on Gold in Electrolyte Solutions: Adsorbed Sulfur or Gold Sulfide? *J. Phys. Chem C* **2008,** *112*, 11394-11402.

21. Kim, S. T.; Saha, K.; Kim, C.; Rotello, V. M. The Role of Surface Functionality in Determining Nanoparticle Cytotoxicity. *Acc. Chem. Res.* **2013,** *46*, 681-691.

22. Fratoddi, I.; Venditti, I.; Cametti, C.; Russo, M. V. How Toxic are Gold Nanoparticles? The State-of-the-art. *Nano Res.* **2015,** *8*, 1771-1799.

23. Jiao, P. F.; Zhou, H. Y.; Chen, L. X.; Yan, B. Cancer-Targeting Multifunctionalized Gold Nanoparticles in Imaging and Therapy. *Curr. Med. Chem.* **2011,** *18*, 2086-2102.

24. Yang, S.-T.; Liu, Y.; Wang, Y.-W.; Cao, A. Biosafety and Bioapplication of Nanomaterials by Designing Protein–Nanoparticle Interactions. *Small* **2013,** *9*, 1635-1653.

25. Bogdanov, A. A.; Gupta, S.; Koshkina, N.; Corr, S. J.; Zhang, S.; Curley, S. A.; Han, G. Gold Nanoparticles Stabilized with MPEG-Grafted Poly(l-lysine): in Vitro and in Vivo Evaluation of a Potential Theranostic Agent. *Bioconj. Chem.* **2015,** *26*, 39-50.

26. Grabar, K. C.; Freeman, R. G.; Hommer, M. B.; Natan, M. J. Preparation and Characterization of Au Colloid Monolayers. *Anal. Chem.* **1995,** *67*, 735-743.

27. Ravel, B.; Newville, M. ATHENA, ARTEMIS, HEPHAESTUS: Data Analysis for X-ray Absorption Spectroscopy Using IFEFFIT. *J. Synchrotron Radiat.* **2005,** *12*, 537-541.

28. Abbate, M.; Vicentin, F. C.; Compagnon-Cailhol, V.; Rocha, M. C.; Tolentino, H. The Soft X-ray Spectroscopy Beamline at the LNLS: Technical Description and Commissioning Results. *J. Synchrotron Radiat.* **1999,** *6*, 964-972.

29. Vairavamurthy, A. Using X-ray Absorption to Probe Sulfur Oxidation States in Complex Molecules. *Spectrochim. Acta: Molec. Biomolec. Spectrosc.* **1998,** *54*, 2009-2017.

30. Zweifel, D. A.; Wei, A. Sulfide-Arrested Growth of Gold Nanorods. *Chem. Mater.s* **2005,** *17*, 4256-4261.

31. Guinier, A.; Fournet, G. *Small-Angle Scattering of X-rays*. John Wiley: New York, 1955.

32. Averitt, R. D.; Westcott, S. L.; Halas, N. J. Linear Optical Properties of Gold Nanoshells. *J. Opt. Soc. Am. B* **1999,** *16*, 1824-1832.

33. Kirkland, A. I.; Jefferson, D. A.; Duff, D. G.; Edwards, P. P.; Gameson, I.; Johnson, B. F. G.; Smith, D. J. Structural Studies of Trigonal Lamellar Particles of Gold and Silver. *Proc. R. Soc. Lond. Series A: Math. Phys. Sci.* **1993,** *440*, 589.

34. Sánchez-Iglesias, A.; Pastoriza-Santos, I.; Pérez-Juste, J.; Rodríguez-González, B.; García de Abajo, F. J.; Liz-Marzán, L. M. Synthesis and Optical Properties of Gold Nanodecahedra with Size Control. *Adv. Mater.* **2006,** *18*, 2529-2534.

35. Ishikawa, K.; Isonaga, T.; Wakita, S.; Suzuki, Y. Structure and Electrical Properties of Au_2S. *Solid State Ionics* **1995,** *79*, 60-66.

36. Tan, M. C.; Ying, J. Y.; Chow, G. M. Composition, Particle Size, and Near-infrared Irradiation Effects on Optical Properties of Au–Au_2S Nanoparticles. *J. Mater. Res.* **2008,** *23*, 281-293.

37. Finkelstein, N. P.; Hancock, R. D. A New Approach to the Chemistry of Gold. *Gold Bull.* **1974,** *7*, 72-77.

38. Mikhlin, Y.; Romanchenko, A.; Likhatski, M.; Karacharov, A.; Erenburg, S.; Trubina, S. Understanding the Initial Stages of Precious Metals Precipitation: Nanoscale Metallic and Sulfidic Species of Gold and Silver on Pyrite Surfaces. *Ore Geol. Rev.* **2011,** *42*, 47-54.

39. Ramallo-López, J. M.; Giovanetti, L. J.; Requejo, F. G.; Isaacs, S. R.; Shon, Y. S.; Salmeron, M. Molecular Conformation Changes in Alkylthiol Ligands as a Function of Size in Gold Nanoparticles: X-ray Absorption Studies. *Phys. Rev. B* **2006,** *74*, 073410.

40. Guerrero, E.; Rojas, T. C.; Multigner, M.; Crespo, P.; Muñoz-Márquez, M. A.; García, M. A.; Hernando, A.; Fernández, A. Evolution of the Microstructure, Chemical Composition and Magnetic Behaviour During the Synthesis of Alkanethiol-capped Gold Nanoparticles. *Acta Mater.* **2007,** *55*, 1723-1730.

41. Biener, M. M.; Biener, J.; Friend, C. M. Revisiting the S−Au(111) Interaction: Static or Dynamic? *Langmuir* **2005,** *21*, 1668-1671.

42. Kleinjan, W. E.; Keizer, A. d.; Janssen, A. J. H. Kinetics of the Chemical Oxidation of Polysulfide Anions in Aqueous Solution. *Water Res.* **2005,** *39*, 4093-4100.

43. Vairavamurthy, A.; Manowitz, B.; Luther, G. W.; Jeon, Y. Oxidation State of Sulfur in Thiosulfate and Implications for Anaerobic Energy Metabolism. *Geochim. Cosmochim. Acta* **1993,** *57*, 1619-1623.

44. Almkvist, G.; Boye, K.; Persson, I. K-edge XANES Analysis of Sulfur Compounds: an Investigation of the Relative Intensities Using Internal Calibration. *J. Synchrotron Radiat.* **2010,** *17*, 683-688.

45. Jalilehvand, F. Sulfur: Not a "Silent" Element Any More. *Chem. Soc. Rev.* **2006,** *35*, 1256-1268.

46. Pensa, E.; Cortés, E.; Corthey, G.; Carro, P.; Vericat, C.; Fonticelli, M. H.; Benítez, G.; Rubert, A. A.; Salvarezza, R. C. The Chemistry of the Sulfur–Gold Interface: In Search of a Unified Model. *Acc. Chem. Res.* **2012,** *45*, 1183-1192.

47. Yu, M.; Ascolani, H.; Zampieri, G.; Woodruff, D. P.; Satterley, C. J.; Jones, R. G.; Dhanak, V. R. The Structure of Atomic Sulfur Phases on Au(111). *J. Phys. Chem C* **2007,** *111*, 10904-10914.

48. Abufager, P. N.; Zampieri, G.; Reuter, K.; Martiarena, M. L.; Busnengo, H. F. Long-Range Periodicity of S/Au(111) Structures at Low and Intermediate Coverages. *J. Phys. Chem C* **2014,** *118*, 290-297.

49. Rodriguez, J. A.; Dvorak, J.; Jirsak, T.; Liu, G.; Hrbek, J.; Aray, Y.; González, C. Coverage Effects and the Nature of the Metal−Sulfur Bond in S/Au(111): High-Resolution Photoemission and Density-Functional Studies. *J. Am. Chem. Soc.* **2003,** *125*, 276-285.

50. Cotton, F. A.; Wilkinson, G.; Murillo, C. A.; Bochmann, M. *Advanced Inorganic Chemistry: A Comprehensive Text*. 6th ed.; Wiley-Interscience: New York, 1999.

51. Buckley, A. N.; Hamilton, I. C.; Woods, R. An Investigation of the Sulphur(−II)/Sulphur(0) System on Gold Electrodes. *J. Electroanal. Chem. Interfacial Electrochem.* **1987,** *216*, 213-227.

52. Charchar, P.; Christofferson, A. J.; Todorova, N.; Yarovsky, I. Understanding and Designing the Gold–Bio Interface: Insights from Simulations. *Small* **2016,** *12*, 2395-2418.

53. Nel, A.; Xia, T.; Meng, H.; Wang, X.; Lin, S.; Ji, Z.; Zhang, H. Nanomaterial Toxicity Testing in the 21st Century: Use of a Predictive Toxicological Approach and High-Throughput Screening. *Acc. Chem. Res.* **2013,** *46*, 607-621.

54. Hak, S.; Helgesen, E.; Hektoen, H. H.; Huuse, E. M.; Jarzyna, P. A.; Mulder, W. J. M.; Haraldseth, O.; Davies, C. d. L. The Effect of Nanoparticle Polyethylene Glycol Surface Density on Ligand-Directed Tumor Targeting Studied in Vivo by Dual Modality Imaging. *ACS Nano* **2012,** *6*, 5648-5658.

55. Vigderman, L.; Zubarev, E. R. Therapeutic Platforms Based on Gold Nanoparticles and their Covalent Conjugates with Drug Molecules. *Adv. Drug Deliv. Rev.* **2013,** *65*, 663-676.

56. Pissuwan, D.; Niidome, T.; Cortie, M. B. The Forthcoming Applications of Gold Nanoparticles in Drug and Gene Delivery Systems. *J. Control. Release* **2011,** *149*, 65-71.

57. Link, S.; Mohamed, M. B.; El-Sayed, M. A. Simulation of the Optical Absorption Spectra of Gold Nanorods as a Function of Their Aspect Ratio and the Effect of the Medium Dielectric Constant. *J. Phys. Chem B* **1999,** *103*, 3073-3077.

58. Liu, X.; Atwater, M.; Wang, J.; Huo, Q. Extinction Coefficient of Gold Nanoparticles with Different Sizes and Different Capping Ligands. *Colloids Surf. B* **2007,** *58*, 3-7.

59. Liu, W.-L.; Lin, F.-C.; Yang, Y.-C.; Huang, C.-H.; Gwo, S.; Huang, M. H.; Huang, J.-S. The Influence of Shell Thickness of Au@TiO_2 Core-shell Nanoparticles on the Plasmonic Enhancement Effect in Dye-Sensitized Solar Cells. *Nanoscale* **2013,** *5*, 7953-7962.

60. Petrova, H.; Perez Juste, J.; Pastoriza-Santos, I.; Hartland, G. V.; Liz-Marzan, L. M.; Mulvaney, P. On the Temperature Stability of Gold Nanorods: Comparison Between Thermal and Ultrafast Laser-induced Heating. *Phy. Chem. Chem. Phys.* **2006,** *8*, 814-821.

61. Li, F.; Zhang, H.; Dever, B.; Li, X.-F.; Le, X. C. Thermal Stability of DNA Functionalized Gold Nanoparticles. *Bioconj. Chem.* **2013,** *24*, 1790-1797.

62. Osinkina, L.; Carretero-Palacios, S.; Stehr, J.; Lutich, A. A.; Jäckel, F.; Feldmann, J. Tuning DNA Binding Kinetics in an Optical Trap by Plasmonic Nanoparticle Heating. *Nano Lett.* **2013,** *13*, 3140-3144.

63. Templeton, A. C.; Hostetler, M. J.; Kraft, C. T.; Murray, R. W. Reactivity of Monolayer-Protected Gold Cluster Molecules: Steric Effects. *J. Am. Chem. Soc.* **1998,** *120*, 1906-1911.

64. Hostetler, M. J.; Templeton, A. C.; Murray, R. W. Dynamics of Place-Exchange Reactions on Monolayer-Protected Gold Cluster Molecules. *Langmuir* **1999,** *15*, 3782-3789.

65. Reimers, J. R.; Ford, M. J.; Halder, A.; Ulstrup, J.; Hush, N. S. Gold Surfaces and Nanoparticles are Protected by Au(0)–thiyl Species and are Destroyed when Au(I)–thiolates Form. *Proc. Natl. Acad. Sci. USA* **2016,** *113*, E1424-E1433.

TABLE OF CONTENTS

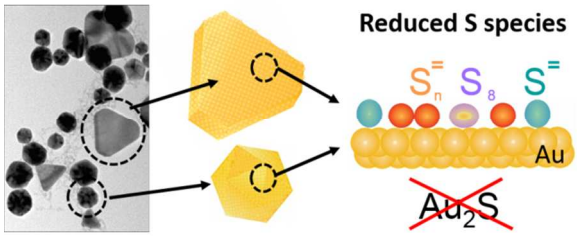

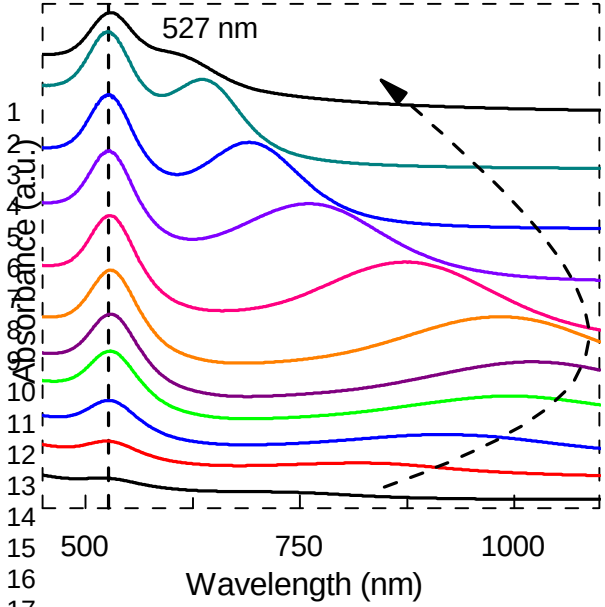
527 nm
Absorbance (a.u.)
500
750
1000
Wavelength (nm)

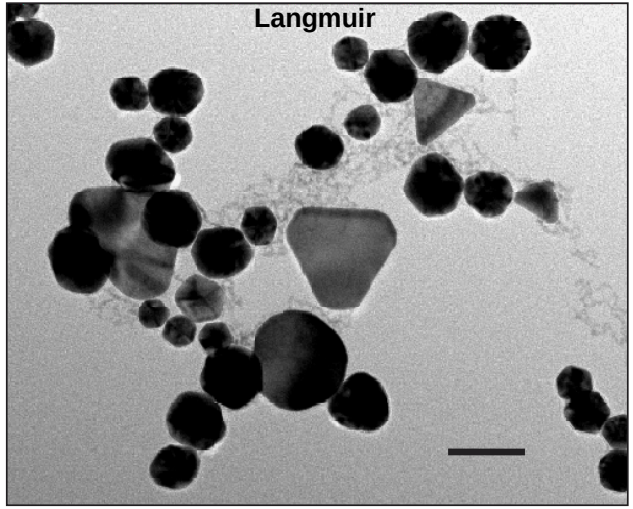
Langmuir

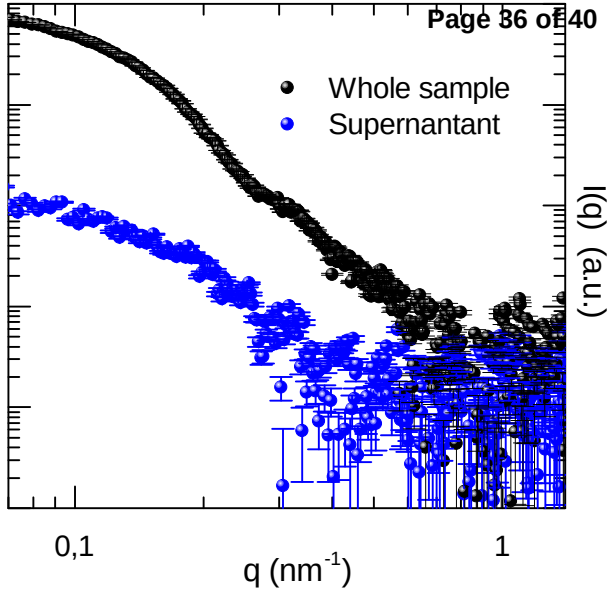
Whole sample
Supernantant
I(q) (a.u.)
0,1
1
q (nm-1)

a)

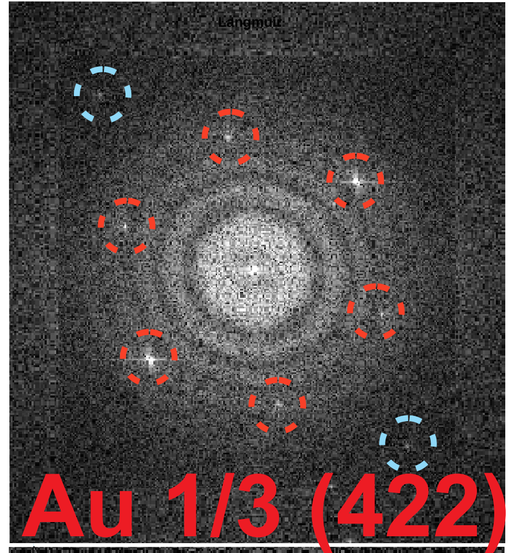

b)

c)

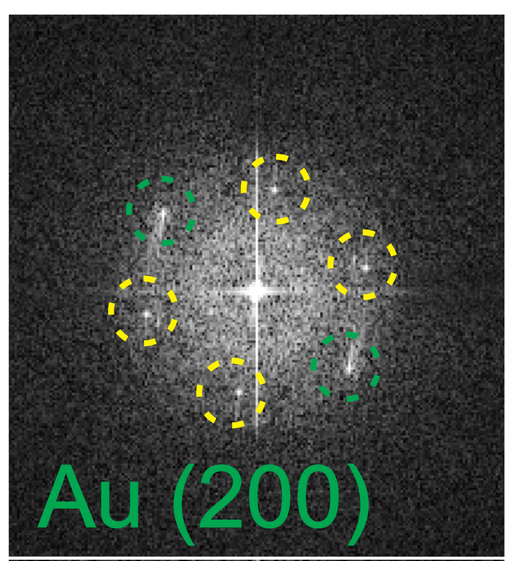

d)

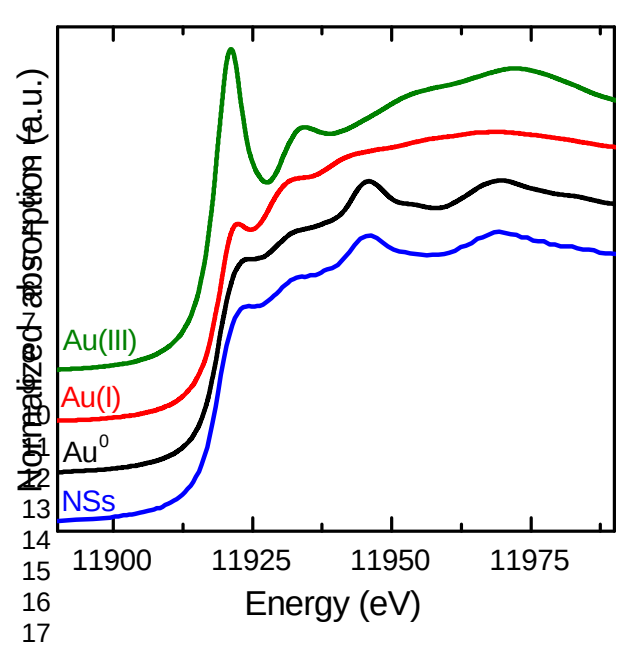

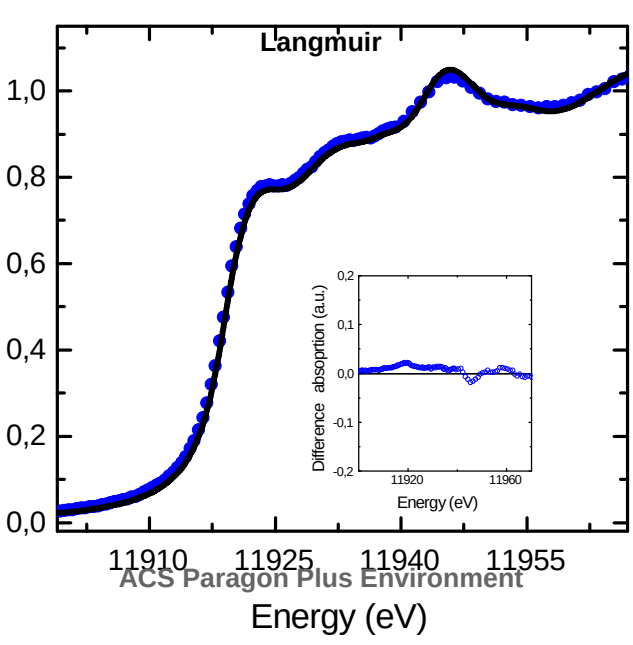

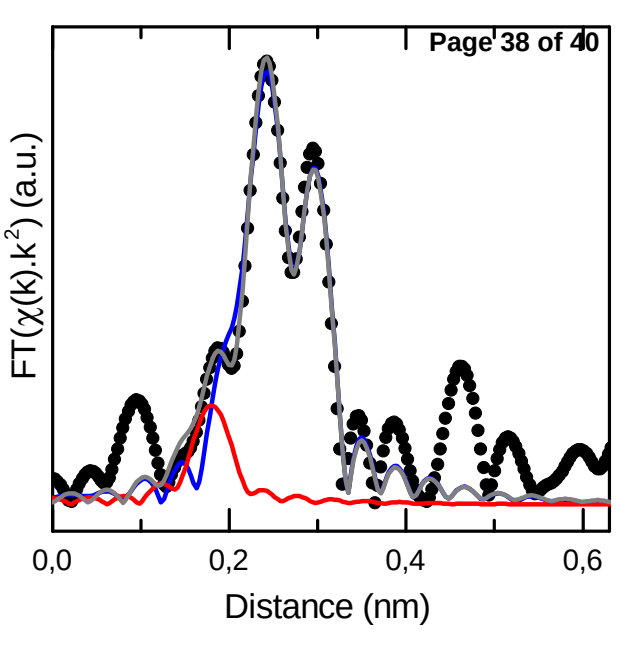

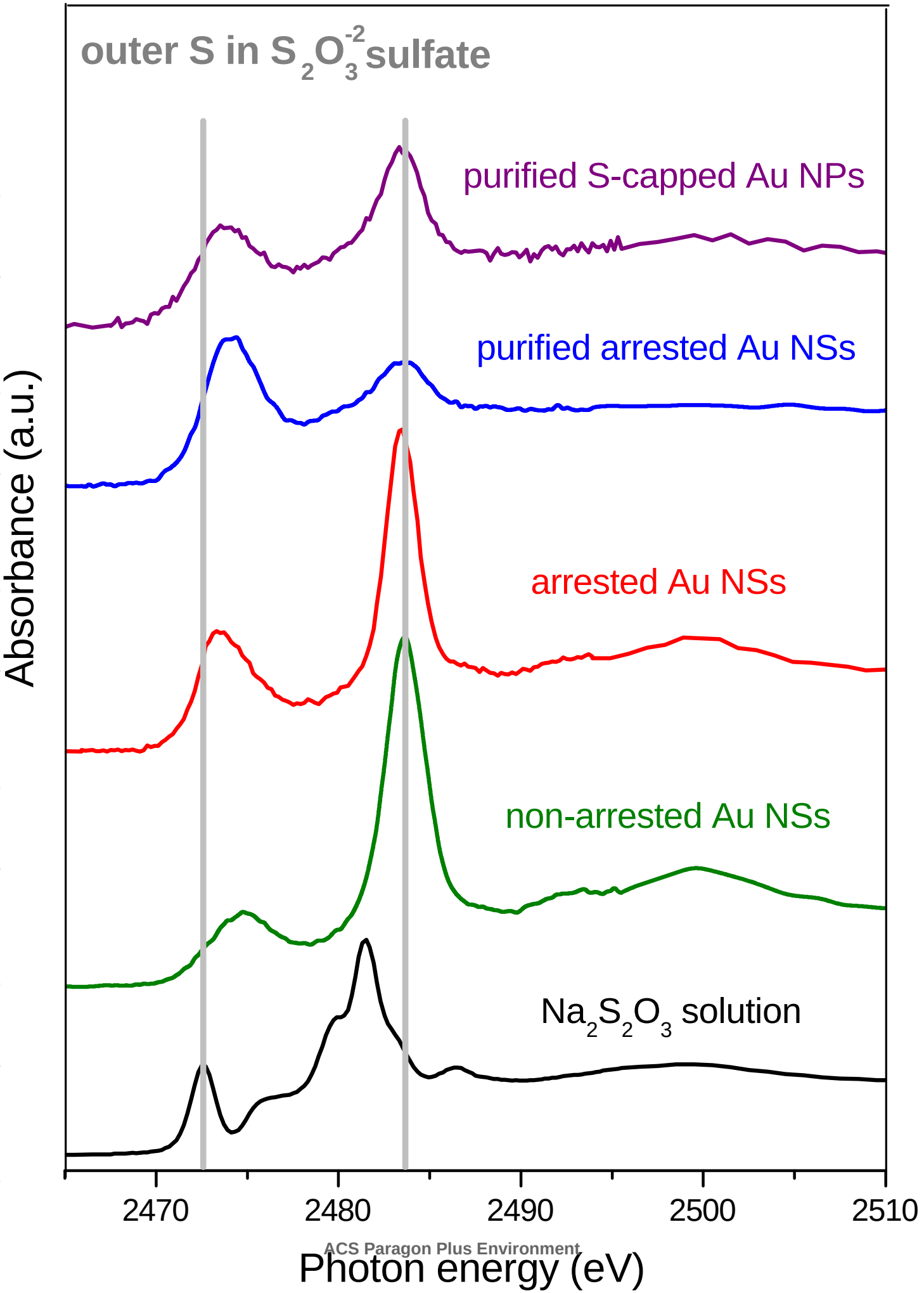
outer S in $S_2O_3^{-2}$ sulfate
purified S-capped Au NPs
purified arrested Au NSs
arrested Au NSs
non-arrested Au NSs
$Na_2S_2O_3$ solution
Absorbance (a.u.)
2470
2480
2490
2500
2510
Photon energy (eV)